Reaction rate for carbon burning in massive stars

C.L. Jiang[1], D. Santiago-Gonzalez[2,1], S. Almaraz-Calderon[1,3], K.E. Rehm[1], B.B. Back[1], K. Auranen[1], M.L. Avila[1], A.D. Ayangeakaa[1], S. Bottoni[1], M.P. Carpenter[1], C. Dickerson[1], B. DiGiovine[1], J.P. Greene[1], C.R. Hoffman[1], R.V.F. Janssens[1], B.P. Kay[1], S.A. Kuvin[4,1], T. Lauritsen[1], R.C. Pardo[1], J. Sethi[5,1], D. Seweryniak[1], R. Talwar[1], C. Ugalde[1], S. Zhu[1], D. Bourgin[6], S. Courtin[6,7], F. Haas[6], M. Heine[6], G. Fruet[6], D. Montanari[6], D.G Jenkins[8], L. Morris[8], A. Lefebvre-Schuhl[9], M. Alcorta[10], X. Fang[11], X.D. Tang[12], B. Bucher[13], C.M. Deibel[2], and S.T. Marley[2]

[1] *Physics Division, Argonne National Laboratory, Argonne, IL 60439, USA*
[2] *Department of Physics and Astronomy, Louisiana State University, Baton Rouge, LA70803, USA*
[3] *Department of Physics, Florida State University, Tallahassee, FL 32306, USA*
[4] *Department of Physics, University of Connecticut, Storrs, CT06269, USA*
[5] *Department of Chemistry and Biochemistry, University of Maryland, College Park, MD20742, USA*
[6] *IPHC and CNRS, Universite de Strasbourg, F-67037 Strasbourg, France*
[7] *USIAS, F-67083 Strasbourg, France*
[8] *Department of Physics,University of York, Heslington, York YO10 5DD, UK*
[9] *IN2P3-CNRS and University of Paris Sud, F-91405 Orsay-campus, France*
[10] *TRIUMF, Vancouver, BC V6T 2A3, Canada*
[11] *Sino-French Institute of Nuclear Engineering and Technology, Sun Yat-Sen University, Zhuhai 519082, PR China*
[12] *Institute of Modern Physics, Lanzhou, PR China and*
[13] *Lawrence Livermore National Laboratory, Livermore, CA 94551, USA*

(Dated: November 20, 2017)

Carbon burning is a critical phase for nucleosynthesis in massive stars. The conditions for igniting this burning stage, and the subsequent isotope composition of the resulting ashes, depend strongly on the reaction rate for ^{12}C + ^{12}C fusion at very low energies. Results for the cross sections for this reaction are influenced by various backgrounds encountered in measurements at such energies. In this paper, we report on a new measurement of ^{12}C+^{12}C fusion cross sections where these backgrounds have been minimized. It is found that the astrophysical S factor exhibits a maximum around E_{cm}=3.5 - 4.0 MeV which leads to a reduction of the previously predicted astrophysical reaction rate.

PACS numbers: 25.70.Jj, 26.30.-k, 24.10.Eq, 24.30.Gd

When a massive star has exhausted its supply of hydrogen and helium, it contracts under gravitational pressure, leading to an increase in temperature. At these elevated temperatures, the ashes of helium burning (i.e., ^{12}C) can ignite and initiate the so-called carbon burning phase [1, 2]. The ^{12}C + ^{12}C fusion reaction is an important route for the production of elements with mass A$\geq$20, and it also influences the subsequent nucleosynthesis processes via slow and rapid neutron-capture reactions [3].

In explosive scenarios such as in type Ia supernovae, carbon burning occurs at higher temperatures. While experimental data, relevant for this energy regime can be found in the literature [4–11], the associated Gamow energies are still quite low, resulting in small cross sections which are in many cases difficult to measure because of contributions from background reactions. Furthermore, as discussed in Ref. [9], there are 20-100 keV energy shifts between the excitation functions measured by different groups resulting in large variations of the ^{12}C + ^{12}C fusion cross sections.

For quiescent carbon burning in massive stars, the Gamow window is so low that no experimental data exist in this energy regime. Phenomenonological extrapolations or model calculations are, therefore, needed in order to obtain the astrophysical reaction rate of the ^{12}C + ^{12}C reaction. For this extrapolation, several predictions can be found in the literature [12–15].

A summary of the experimental data found in the literature is given in Fig. 1 as a plot of the S factor vs. E_{cm} ($S(E_{cm}) = \sigma E_{cm} e^{2\pi\eta}$) [4–11], where E_{cm} is the center-of-mass energy, σ is the fusion cross section and η is the Sommerfeld parameter. The Gamow energy associated with quiescent carbon burning in massive stars is less than 2 MeV, outside the energy region in Fig. 1 [16].

As can be seen in Fig. 1, the experimental S factors in the energy region of $E_{cm} \sim$ 3-4 MeV differ by up to one order of magnitude. The two most recent experiments, by Spillane *et al.* [10] and by Zickefoose *et al.* [11], shown in Fig. 1 by the magenta and green symbols respectively, used two different detection techniques. In Ref. [10], the γ rays of the evaporation residues were detected, while Ref. [11] measured the charged particles emitted by the evaporation residues. The large uncertainties in these two experiments at the lowest energies are caused by the background encountered by the detection techniques and by the thick-target method which requires the subtraction of two spectra taken at slightly different energies. While Ref. [10] claimed to have observed a resonance at about 2.14 MeV, the later measurement [11] obtained cross sections in the same energy region smaller by about two orders of magnitude.

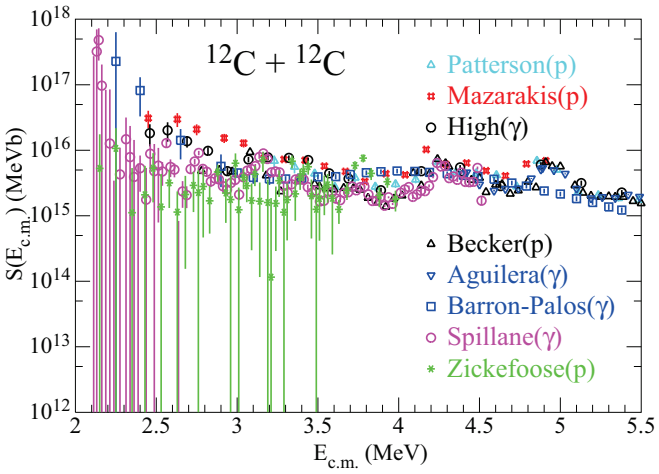

FIG. 1: (Color) S factors from previous measurements of the ^{12}C + ^{12}C fusion reaction. Charged-particle detection was used in the measurements by Patterson, Mazarakis, Becker and Zickefoose, while γ-ray detection was employed in the measurements of High, Barron-Palos, Auguilera and Spillane [4–11].

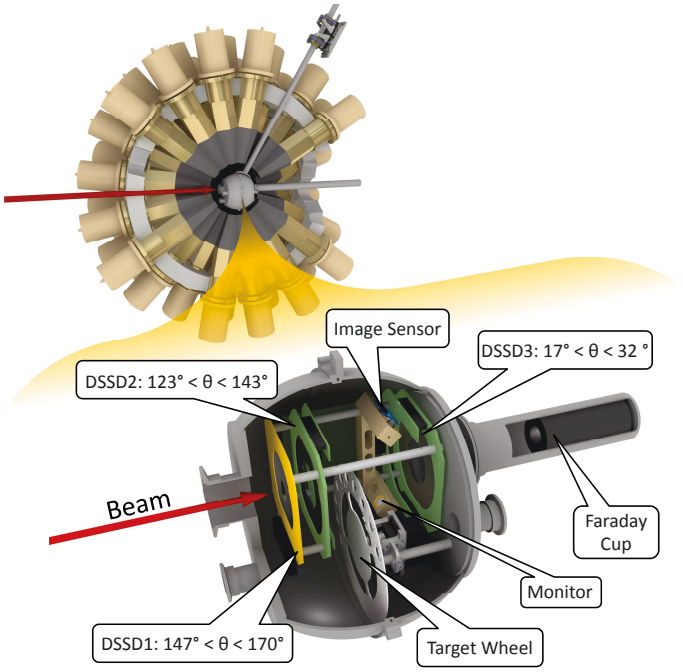

FIG. 2: (Color online) A schematic drawing of the experimental setup showing the spherical target chamber mounted in the middle of the Gammasphere array.

In order to obtain more reliable cross sections of ^{12}C + ^{12}C fusion at low energies, a reduction of the background is essential. For this purpose, we have developed a particle-γ coincidence technique that minimizes these backgrounds and provides reliable fusion cross sections for the ^{12}C + ^{12}C system [17]. In this article, we present results from measurements using this technique and discuss their impact on the astrophysical reaction rates of carbon burning and on the theory of fusion reactions.

The experiment was performed at the ATLAS accelerator at Argonne National Laboratory using Gammasphere in coincidence with silicon detectors. Gammasphere is an array of about 100 Compton-suppressed Ge spectrometers [18], which detect the γ rays from the ^{20}Ne and ^{23}Na evaporation residues. The coincident charged particles emitted from the compound nuclei were identified in a compact array of three annular silicon detectors (DSSD1, DSSD2 and DSSD3) located inside the target chamber. A schematic drawing of the experimental setup is provided in Fig. 2. Each Si detector had a thickness of 500 μm and was subdivided into 16 rings and 16 wedges covering the angular ranges of 147-170°, 123-143° and 17-32°, respectively. The total solid angle coverage was about 25% of 4π. In order to reduce the random coincident events, aluminum-absorber foils of different thickness were placed in front of the DSSD's to reduce the count rate from elastically scattered ^{12}C ions and, in some cases, from background reactions (*e.g.,* ^{12}C + ^{1}H $\rightarrow$ p and ^{12}C + ^{2}H $\rightarrow$ p or d). A Faraday cup and two monitor detectors were used for beam normalization. In addition, an image sensor sensitive to infrared light was installed to monitor the beam spot size and location during the experiment. Contrary to the measurements in Ref. [10, 11], this is a thin-target experiment which does not require the subtraction of spectra taken at different energies.

Isotopically enriched ($\geq$ 99.9%) ^{12}C targets with thickness of about 30-50 μg/cm^2 were used. In order to correct the cross sections for transitions populating the ground states and several high-lying states in ^{23}Na and ^{20}Ne and for the limited angular coverage of the DSSDs, we have used the previously measured yields from charged-particles experiments by Becker *et al.* and Mazarakis *et al.*, [5, 7]. Similar corrections have been made in previous γ-ray [8] or charged-particles experiments [11].

Measurements were performed at ten beam energies between E_{lab}=5.5-10 MeV, with maximum beam currents of about 600 pnA. The beam energy for each measurement was determined using a split-pole magnetic spectrograph, which was calibrated with standard α sources. A detailed description of the experiment and the resulting reduction in background using the particle-γ coincidence technique can be found in Ref. [17].

Particle-γ coincidence events from the ^{12}C(^{12}C,p)^{23}Na fusion reaction populating the first excited state (^{23}Na$_{1st}$) in ^{23}Na at an excitation energy E_x=0.440 MeV measured in DSSD1 at the second lowest energy, E_{cm}=2.84 MeV, are displayed in Figs. 3a and 3b. The 440-keV γ rays emitted from the fusion evaporation residues ^{23}Na$_{1st}$ in coincidence with protons, p_1 of energies of $\sim$ 2.2 MeV, are located in the rectangular region in Fig. 3a. In a plot of scattering angle vs. particle energy, these events follow the kinematics expected for the ^{12}C(^{12}C,p$_1$)^{23}Na$_{1st}$ reaction, as indicated by the dashed

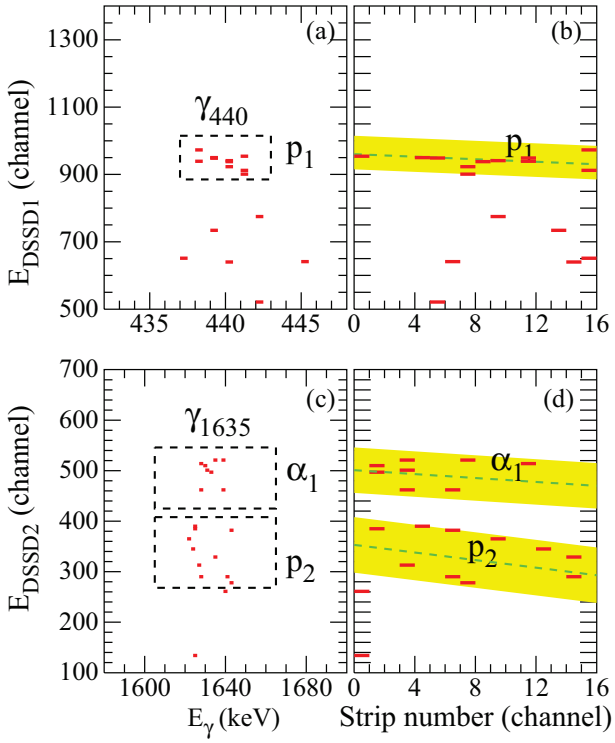

FIG. 3: (Color online) (a) Particle-γ coincidence events detected by DSSD1 located at backward angles at the second lowest energy studied in this experiment, E_{cm}=2.84 MeV; (b) Energy-angle correlation of the coincident particle-γ events shown in the rectangular region in Fig. 3b. The dashed line represents the kinematic locus expected for the ^{12}C(^{12}C,p)^{23}Na reaction populating the 0.440-MeV state in ^{23}Na; (c) and (d) plots similar to (a) and (b), but measured for the third lowest energy, E_{cm}=2.96 MeV. The dashed lines represent the kinematic locus expected for the ^{12}C(^{12}C,α)^{20}Ne and ^{12}C(^{12}C,p)^{23}Na reactions. See text for details.

line (and the yellow band) in Fig. 3b.

Similar results are obtained for the ^{12}C(^{12}C,α)^{20}Ne reaction by gating on the 1.635-MeV, $2^+ \rightarrow 0^+$ transition in ^{20}Ne, as shown in Figs. (3c) and (3d) for the third lowest energy, E_{cm}=2.96 MeV, measured in DSSD2. As seen in Fig. 3, there are two groups of coincident particles α_1 and p_2 because a γ ray of 1.635 MeV can originate from the decay of the 2^+_1 state in ^{20}Ne which is in coincidence with an α particle, but also from the decay of the $7/2^+_1$ level to the $5/2^+_1$ state in ^{23}Na (E_γ=1.64 MeV), which is in coincidence with a proton, hence showing the high resolving power of the particle-γ-coincidence technique. Bands in Figs. (3b) and (3d) are the regions of good events.

The total coincidence efficiency was determined from the angle coverage of the DSSD's and the efficiency of γ-ray detection. The later one was found to be around 9% for E_γ=440 and 7% for E_γ=1635 keV, respectively. The measured total fusion cross sections are listed in Table I and the measured partial fusion cross sections are givin in the supplemental material [19]. The cross section at 4.93 MeV, 4.8 ± 0.9 mb, is in good agreement with the result of Ref. [8]. It should be noted that the cross sections obtained in the present experiment are values averaged over the energy range by assuming an exponential energy dependence of the cross sections. The uncertainty at the two lowest-energy points is dominated by statistics, while at all the others systematics is the main contributor.

TABLE I: Cross sections and S factors of the ^{12}C + ^{12}C fusion reaction measured in this experiment.

E_{cm}	σ	S factor
MeV	mb	10^{15}MeVb
4.93 ± 0.07	4.8 ± 0.9	2.8 ± 0.5
4.80 ± 0.07	2.0 ± 0.4	1.9 ± 0.4
4.73 ± 0.07	0.88 ± 0.17	1.1 ± 0.2
4.53 ± 0.07	0.92 ± 0.18	2.6 ± 0.5
4.22 ± 0.08	0.50 ± 0.10	6.0 ± 1.2
3.93 ± 0.08	0.070 ± 0.014	3.6 ± 0.7
3.43 ± 0.08	(4.1 ± 0.8)10^{-3}	4.0 ± 0.8
2.96 ± 0.08	(9.5 ± 1.9)10^{-5}	3.0 ± 0.6
2.84 ± 0.08	(4.0 ± 2.0)10^{-5}	3.5 ± 1.8
2.68 ± 0.08	(6.2 ± 3.1)10^{-6}	2.3 ± 1.2

The astrophysical S factors, calculated from the cross sections measured in this experiment, are shown by the black circles in Fig. 4. They are in good agreement with recent measurements using γ detection [10] and charged particle detection [11] , but have smaller uncertainties.

Four results of model calculations and extrapolations into the low-energy region are included in Fig. 4 as well. The earliest extrapolation from Fowler and Caughlan is given by the light-blue curve [12]. Esbensen *et al.,* calculated the cross sections in this energy region with the so-called sudden model (magenta-dashed curve) [14]. It was pointed out in Ref. [15] that, for the fusion reaction of ^{12}C + ^{12}C $\rightarrow$ ^{24}Mg, the level density in the compound nucleus ^{24}Mg is low and the level widths are small. Therefore, the conditions for using the incoming wave boundary condition in the coupled-channels (CC) calculations are not fulfilled. A calculation where this correction was included [15] is presented in Fig. 4 as the black curve (corrected).

The S factors from these three extrapolations increase with decreasing energy, contrary to the extrapolation which is based on the so-called hindrance recipe, described in Ref. [13] (red curve in Fig. 4):

$$\sigma(E) = \sigma_s \frac{E_s}{E} e^{[A_0(E-E_s) - B_0 \frac{2}{E_s^{0.5}}[(\frac{E_s}{E})^{0.5}-1]]}, \qquad (1)$$

where σ_s, E_s, A_0 and B_0 are fit parameters. σ_s and E_s are the cross section and energy at the $S(E)$-factor maximum. This extrapolation will be discussed in more detail below.

In the region of the lowest energies measured in this experiment, our data do not agree with the increase of the S factor predicted by Fowler ([12]), Esbensen (Sudden, [14]) and Jiang (Corrected, [15]). Instead, we note that the S factor appears to decline towards the lower

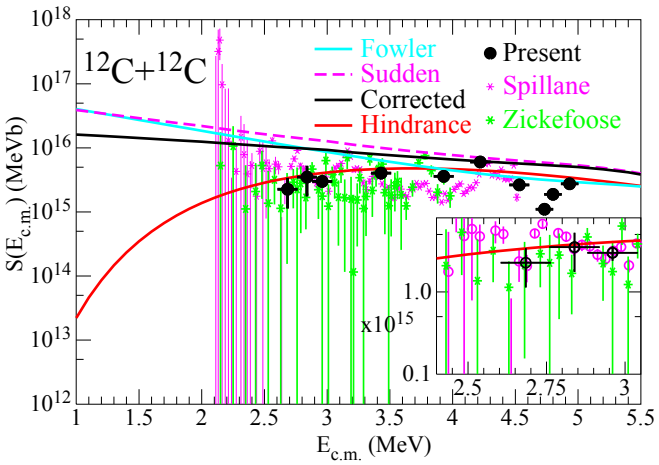

FIG. 4: (Color) Black points: S factors from the present measurements of the ^{12}C + ^{12}C fusion reaction. Green open circles and magenta stars: results from the recent measurement of the same system in Refs. [10] and [11], respectively. The insert gives an enlarged plot in the region near 2.7 MeV. The light blue, magenta-dashed, black and red lines are calculations explained in the text.

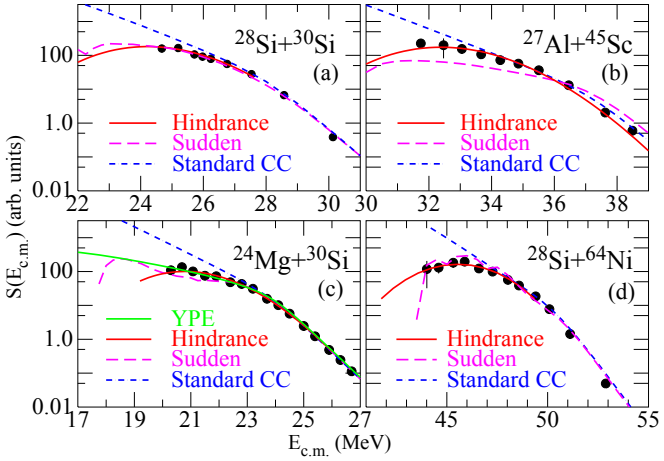

FIG. 5: (Color online) S factors for the systems ^{28}Si + ^{30}Si (a), ^{27}Al + ^{45}Sc (b), ^{24}Mg + ^{30}Si (c), and ^{28}Si + ^{64}Ni (d). The fusion Q-values are 14.3, 9.63, 17.89 and -1.87 MeV, respectively. The various lines are the result of calculations discussed in the text.

energy region of the present measurement and exhibits a weak maximum around 3.5 - 4 MeV, a behavior similar to the hindrance phenomenon found ten years ago in reactions between medium mass nuclei [20, 21]. Here it was observed that, at low energies, the fusion cross sections fall off faster than expected by CC calculations using standard Woods-Saxon potentials. This steep fall-off produces a maximum in the S factor at low energies. Since, for medium-mass systems, the fusion Q values are usually negative, there has to be an S-factor maximum because $\sigma = 0$ at energies $E \leq -Q$ [22]. For these systems, the maximum of the S factor occurs typically at excitation energies of the compound system of 20-40 MeV.

Two approaches have been proposed to describe the occurence of fusion hindrance at low energies. In the 'sudden model', Mişicu and Esbensen [23] introduced a repulsive core in the interaction potential to describe the saturation properties of nuclear matter. Ichikawa *et al.* [24] developed an adiabatic model to explain the fusion hindrance by introducing a damping factor for the coupling strength in the region where the two colliding partners come into contact.

More recently, fusion hindrance has also been studied for systems with positive Q values. Contrary to fusion reactions with negative Q values, these systems do not require the presence of a maximum in the S factor since, even at $E = 0$, the fusion cross section can have a finite value. Some examples are presented in Fig. 5 [25–28] for the systems ^{28}Si + ^{30}Si, ^{27}Al + ^{45}Sc and ^{24}Mg + ^{30}Si [25] with positive fusion Q values (Q=14.3, 9.63 and 17.89 MeV, respectively), while for ^{28}Si + ^{64}Ni, Fig. 5d, the Q value is negative: -1.78 MeV.

Three kinds of calculations and extrapolations are included in Fig. 5. The blue dash-dotted curves are CC calculations with a standard Woods-Saxon potential, which always overpredict the experimental data at low energies. The magenta-dashed curves are CC calculations with a repulsive core included in the potential (sudden model), while the red curves are from the empirical extrapolations (hindrance, [13]) using the same recipe as for the red line in Fig. 4. For these medium-mass systems, the calculations based on the sudden model reproduce the experimental data quite well, as can be seen from the magenta-dashed lines.

This, however, is not the case for the ^{12}C + ^{12}C system which exhibits a broad, but noticeable maximum in the S factor around 3.5 - 4 MeV. The shape of the excitation function shown by the black points in Fig. 4 is similar to the ones presented in Fig. 5, indicating the presence of fusion hindrance in this system. However, sudden model calculations including a repulsive core [14], (magenta dashed line in Fig. 4) indicate an increase of the S factor towards lower energies, in disagreement with the experimental data. Over the energy range of the present measurement, the red curve which was based on the systematics from heavier systems (Ref. [13]) (with parameters, $\sigma_s = 2.3\text{x}10^{-2}$ mb, $E_s = 3.68$ MeV, $A_0 = -1.32$ MeV^{-1} and $B_0 = 52.93$ MeV$^{1/2}$, respectively) appears to agree better than the other extrapolations with the three sets of data discussed here, although additional data are clearly needed in order to determine its validity at even lower energies.

Using the system dependence of these fit parameters as described in Refs. [13, 25–27], one obtaines the red lines of Figs. 4 and 5a-5c, which are in good agreement with experimental data, including those for the ^{12}C + ^{12}C system, where all previous extrapolations predict an increase towards lower energies that is at variance with the new data.

To illustrate that the present data can be well repro-

duced by the the hindrance recipe (red curve), comparisons of χ^2-values for the three data sets (Spillane *et al.*, Zickefoose *et al.*, and the present result) with three extrapolation recipes are shown in Table II where the χ^2-values are defined as:

$$\chi^2 = \sum_{i=1}^{n} [(S_i^{ext} - S_i)/\Delta S_i]^2/n. \quad (2)$$

Here, S_i^{ext}, $S_i \pm \Delta S_i$ are the extrapolated and experimental S-factors and their uncertainties, and n is the number of data in each set. In this comparison the sum in Eq. (2) extends over the energy region $E = 2.68 - 3.98$ MeV which is covered by all three experiments. For all three data sets, the hindrance recipe shows the smallest deviations between data and extrapolations. That is, even the fusion data of Spillane *et al.*, [10] and Zickefoose *et al.*, [11] do not support extrapolation recipes, which lead to an increase of the S factor at low energies. In this energy range the smallest χ^2 value, 1.4, occurs for the present experimental result and the hindrance recipe. In the energy range $E \leq 2.68$ MeV where only data from Refs. [10] and [11] exist, the hindrance recipe again gives the lowest χ^2

The astrophysical reaction rates calculated from the experimental data and the extrapolations in Fig. 4 are plotted in Fig. 6 in the temperature range $T_9 = 0.7 - 2$ GK. For higher energies where no experimental data in Ref. [10, 11] are available, the extrapolated S-factor values of Fowler *et al.,* [12] have been used. As expected the highest rate is obtained from the S-factor parameterization of Fowler *et al.,* [12] (solid blue line), followed by the data of Spillane *et al.,* [10] (magenta shaded region). The rate based on the data of Zickefoose *et al.,* [11] (green shaded region) is at $T_9 = 1$ GK lower than the rate of Ref. [10] by a factor of 5 and in good agreement with the red line which represents the reaction rate based on the hindrance model [13]. The consequences of a reduced astrophysical reaction rate for ^{12}C + ^{12}C fusion, as inferred from our results, have been discussed in Ref. [29]. The astrophysical reaction rate calculated from the S factor shown by the red line in Fig. 4 can be parameterized by the equation

$$R = exp(a_0 + a_1/T + a_2 T + a_3 ln(T)), \quad (3)$$

where R is given in $cm^3 mole^{-1} sec^{-1}$, T is the temperature in GK, $a_0 = -14, a_1 = -6.35, a_2 = -4.94$ and $a_3 = 27.6$. The smaller cross sections and the resulting reduced reaction rates shift the ignition of carbon burning in massive stars to higher temperatures and densities, and also enhance the abundance of long-lived radioisotopes such as ^{26}Al and ^{60}Fe. A higher ^{26}Al yield would be in agreement with observations [30].

The isotope ^{60}Fe ($T_{1/2}$=2.61 My) is of particular interest since its detection in deep-sea sediments [31–33] and on the lunar surface [34] has been associated with recent (∼2.8 My) and close (∼10 pc) supernova explosions in our galaxy. Calculations with a reduced ^{12}C + ^{12}C reaction rate for a $20M_\odot$ star predict an increase in ^{60}Fe by about a factor of two [29] which would influence the calculated time and distance of these events. It should be noted, however, that different nucleosynthesis models indicate similar variations in ^{60}Fe production [35].

TABLE II: Comparison of χ^2 values for three different data sets (by Spillane *et al.*, Zickefoose *et al.*, present result) with three extrapolation recipes (by Fowler [12], corrected-Sudden Model [15] and Hindrance [13]). The χ^2 values are defined in Eq. (2).

Exp.	Fowl. [12]	C.Sudd. [15]	Hind. [13]
Spillane [10]	502	1296	384
Zickefoose [11]	13.1	21.3	4.5
Present	35.7	43.4	1.4

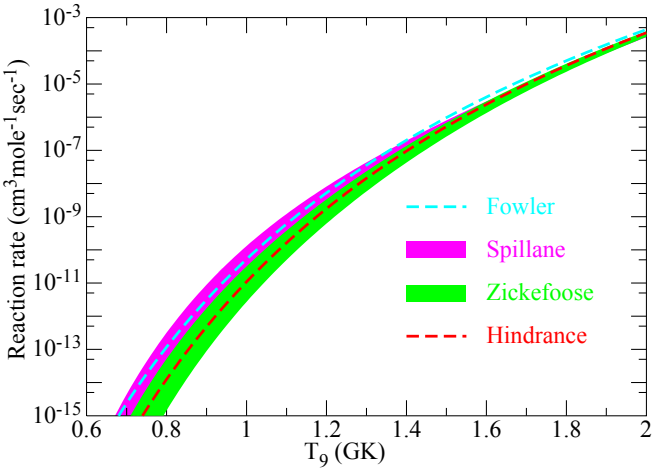

FIG. 6: (Color) Astrophysical reaction rates calculated from the experimental data and extrapolations in Fig. 4. The bands for Spillane and for Zichefoose are made from including their experimental uncertainties, respectively.

In summary, fusion cross sections for ^{12}C + ^{12}C have been measured down to about 6 nb by using a particle-γ coincidence technique, which minimized the backgrounds that plagued earlier experiments. The S factors show a broad maximum indicating the presence of fusion hindrance even for such a light system. Fusion hindrance necessitates a different extrapolation method towards lower energies which leads to smaller astrophysical reaction rates for various astrophysical scenarios and is a challenge to fusion reaction theory.

This work was supported by the US Department of Energy, Office of Nuclear Physics, under Contract No. DE-AC02-06CH11357 and uses resources from ANL's ATLAS facility, which is a DOE Office of Science User facility. D.S.G. and C.M.D. acknowledge the support by the same Office of Nuclear Physics, under grant No. DE-FG02-96ER40978.

[1] C.E. Rolf and W.S. Rodney, Cauldrons in the Cosmos (The University of Chicago Press, 1988).
[2] S.G. Ryan, A.J. Norton, Stellar Evolution and Nucleosynthesis (University of Chicago Press, 2010).
[3] M.E. Bennett *et al.,* Nuclear Physics in Astrophysics IV, Journal of Physics: Conference Series **202**, 012023 (2010).
[4] L.J. Patterson, H. Winkler, and C.S. Zaidins, Astrophys. J. **157**, 367 (1969).
[5] M.G. Mazarakis and W.E. Stephens, Phys. Rev. **C 7**, 1280 (1973).
[6] M.D. High and B. Cujec, Nucl. Phys. **A 282**, 181 (1977).
[7] H.W. Becker, K.U. Kettner, C. Rolfs, and H.P. Trautvetter, Z. Phys. **A 303**, 305 (1981).
[8] L. Barron-Palos *et al.,* Nucl. Phys. **A 779**, 318 (2006).
[9] E.F. Aguilera *et al.,* Phys. Rev. **C 73**, 064601 (2006).
[10] T. Spillane *et al.,* Phys. Rev. Lett. **98** 122501 (2007).
[11] J. Zickefoose, Thesis, U. Conn., (2011) or www.lsw.uni-heidelberg.de/nic2010/talks/Strieder.pdf.
[12] W. Fowler, G. Caughlan and B. Zimmerman, Annu. Rev. Astrophys. **13**, 69 (1975); G.R. Caughlan and W.A. Fowler, At. Data Nucl. Data Tables, **40**, 283 (1988).
[13] C.L. Jiang, K.E. Rehm, B.B. Back and R.V.F. Janssens, Phys. Rev. **C 75**, 015803 (2007).
[14] H. Esbensen, X.D. Tang, and C.L. Jiang, Phys. Rev. **C 84**, 064613 (2011).
[15] C.L. Jiang *et al.,* Phys. Rev. Lett. **110,** 072701 (2013).
[16] White paper on Nuclear Astrophysics and Low Energy Nuclear Physics, Ed. H. Schatz and M. Wiescher, Michigan State University, January 31, 2015
[17] C.L. Jiang *et al.,* Nucl. Instru. Meth. **A 682**, 12 (2012).
[18] I.Y. Lee, Nucl. Phys. **A 520**, 641C (1990).
[19] Supplemental material to this article.
[20] C.L. Jiang *et al.,* Phys. Rev. Lett. **89,** 052701 (2002).
[21] B.B. Back, H. Esbensen, C.L. Jiang and K.E. Rehm, Rev. Mod. Phys. **86**, 317 (2014).
[22] C.L. Jiang, H. Esbensen, B.B. Back, R.V.F. Janssens, and K.E. Rehm, Phys. Rev. **C 69,** 014604 (2004).
[23] S. Mişicu and H. Esbensen, Phys. Rev. Lett. **96**, 112701 (2006); Phys. Rev. C **75**, 034606 (2007).
[24] T. Ichikawa, K. Hagino and A. Iwamoto, Phys. Rev. C **75**, 057603 (2007); Phys. Rev. Lett. **103**, 202701 (2009); T. Ichikawa, K. Matsuyanagi, Phys. Rev. C **88**, 011602(R) (2013).
[25] C.L. Jiang *et al.,* Phys. Rev. **C 78,** 017601 (2008).
[26] C.L. Jiang *et al.,* Phys. Rev. **C 81,** 024611 (2010).
[27] C.L. Jiang *et al.,* Phys. Rev. Lett. **113,** 022701 (2014).
[28] C.L. Jiang *et al.,* Phys. Lett. **B 640**, 18 (2006).
[29] L.R. Gasques *et al.,* Phys. Rev. **C 76**, 035802 (2007).
[30] M. Limongi and A. Chieffi, Astrophys. J. **647**, 483 (2006).
[31] K. Knie *et al.,* Phys. Rev. Lett. **83**, 18 (1999).
[32] K. Knie *et al.,* Phys. Rev. Lett. **93**, 171103 (2004).
[33] A. Wallner *et al.,* Nature **532**, 69 (2016).
[34] L. Fimiani *et al.,* Phys. Rev. Lett. **116**, 151104 (2016).
[35] D. Breitschwerdt *et al.,* Nature **532**, 73 (2016).